Various morphologies of nano/micro PbS via green hydrothermal method

Maryam Mohammadikish · Fatemeh Davar ·
Mohammad Reza Loghman-Estarki

Abstract Lead sulfide (PbS) with various morphologies including nanoparticle, microrod, octahedral, cubic, six-armed microstar, dendrite structure and hexagonal disc were synthesized under hydrothermal conditions. The synthesis variables such as the pH of solution, kind of surfactant, reaction temperature and time were observed to influence the final shape of PbS microstructures. The structure and morphology of obtained products were characterized by using X-ray diffraction, Fourier transform infrared spectroscopy, scanning electron microscopy and transmission electron microscopy. UV–Vis spectroscopy showed the direct band gap of ~ 5.8 eV for the PbS microstar that is a large increment compared with that of bulk PbS. The photoluminescence measurements showed that the emission peaks were located at 712 nm. A possible formation mechanism of PbS microcrystals was discussed based on their shape evolutions.

1 Introduction

The morphologies, shapes and sizes of inorganic materials have remarkable effects on their physical and chemical properties [1]. Therefore, developing methods of tailoring the structure to obtain specific morphologies from nanoparticles is recently an interesting subject of many researches.

Lead sulfide (PbS), a special member of the IV–VI semiconductors, has large Bohr's radius (18 nm) indicating strong quantum confinement and narrow band gap (0.41 eV). Its nanoscale counterpart has potential applications in the fields of infrared optoelectronic [2], sensor [3], optical switches [4], thermoelectric devices [5], solar-cells [6] and biotechnology [7]. Hence, the synthesis of PbS micro- and nano-crystals such as microcrystalline tetrapod like structures [8], star-shaped nanocrystals [9], and nanopyramidal films [10] has attracted extensive attention in recent years. Cubic-shaped PbS micro/nanocrystals have been synthesized via the decomposition of a single-source precursor [11] and a solution reflux method [12]. Rod-like PbS nanocrystals have been produced by cation-exchange reactions [13] and combination of surfactant and polymer matrix as a template [14]. Star-shaped PbS microcrystals have been prepared by a solution route [15, 16]. Pyramidal PbS nanocrystals have been obtained at the interface of toluene and water solutions [17]. PbS cubes with a hierarchical pyramidal pit on each face have been formed by a facile template-free solvothermal approach [18]. PbS nanowires [19] and nanosheets [20] have been prepared by solvothermal method. PbS microcrystals with a flower-shaped structure was prepared in a simple aqueous system using microwave irradiation of Pb^{2+} and $S_2O_3^{2-}$ [16].

In present study, nanoparticle, microrod, octahedral, cubic, six-armed microstar, dendrite structure and hexagonal disc PbS have been synthesized by a green synthetic route at mild reaction temperature via simple hydrothermal method. Some factors that affect the morphology of PbS crystals such as pH, kind of surfactant, reaction temperature and time are systematically investigated. The

M. Mohammadikish (✉)
Faculty of Chemistry, Kharazmi University, Tehran, Iran
e-mail: mohammadikish@khu.ac.ir

F. Davar
Department of Chemistry, Isfahan University of Technology, Isfahan, Iran

M. R. Loghman-Estarki
Department of Material Engineering, Malek Ashtar University of Technology, Shahinshahr, Isfahan, Iran

mechanism related to facet-selective growth and dissolution–recrystallization was discussed.

2 Experimental

2.1 Materials and methods

All the chemicals used in this work were of analytical grade and used as received without further purification.

XRD patterns were recorded by a Rigaku D-max C III, X-ray diffractometer using Ni-filtered Cu Kα radiation. Field emission scanning electron microscopy (FESEM) images were obtained on Hitachi. Transmission electron microscopy (TEM) images were obtained on a Philips (EM 208) transmission electron microscope with an accelerating voltage of 100 kV. Fourier transform infrared (FT-IR) spectra were recorded on Rayleigh WQF-510 spectrophotometer in KBr pellets. The electronic spectra of the products were taken on a Bio UV–visible spectrometer (Varian Cary 100). Room temperature photoluminescence (PL) spectra were studied on a F-4500 fluorescence spectrophotometer.

2.2 Synthesis of PbS nanostructures

In a typical procedure, 0.67 g thiourea (tu) in 50 mL H_2O was added to 50 mL aqueous solution containing 0.5 g lead (II) oxalate and 0.35 mL thioglycolic acid (TGA). After stirring for 10 min, the solution was transferred into a 150 mL Teflon-lined stainless steel autoclave. The autoclave was sealed and maintained at various times and temperatures, then cooled to room temperature gradually. Black precipitates of PbS filtered and washed several times with distilled water and ethanol. After that, the product dried in air at 50 °C for 10 h. To study the growth mechanism of the products, the reaction time and temperature, the kind of surfactant [polyethylene glycol (PEG) and TGA] and the pH of the solution were systematically varied.

The details of reaction conditions and morphology evolution of the samples is shown in Table 1.

3 Results and discussion

The hydrothermal reaction is a complicated process, and a variety of factors can influence on the final structure and morphology of the products [21]. The morphology of the PbS microcrystals depends on many reaction factors, including synthesis temperature and time, the kind of surfactant and the pH of reaction. All of the factors are found to be interdependent, thus resulting in PbS microcrystals with different morphologies.

### 3.1 The effect of time, temperature and precursors

The X-ray diffraction patterns were used to determine phase and crystal structure of the as-prepared samples. Figure 1 shows the typical XRD patterns of the as-synthesized PbS products in the presence of TGA (samples 1 and 4). In the low time and temperature (Fig. 1a), the characteristic peaks of PbS were hardly seen. Under this condition, an organic–inorganic composite may be formed that was reported by other researchers [22, 23]. Figure 1b shows the XRD pattern of the as-prepared PbS in 170 °C—18 h. It is clearly revealed that the product has a high degree of crystallinity. All of the peaks match well with the Bragg reflections of the standard face-centered cubic (fcc) structure of PbS crystals [space group: Fm3m (225), JCPDS, 03-0665].

Further morphological analysis of the above samples was carried out using SEM images (Fig. 2). As shown in the SEM images, the PbS microrods with 600–700 nm diameter were formed in the presence of lead (II) oxalate, thiourea and TGA at 110 °C—6 h (Fig. 2a). By increasing the reaction time to 18 h, the octahedral structure of PbS with diameters of about 2 μm could be found (Fig. 2b). From this image it can be seen that the octahedral structure with rough surface is composed of many small PbS subunits (nanocrystals). Further investigation was achieved by increasing the reaction temperature to 140 °C (sample 3 and Fig. 2c, d). As can be seen in Fig. 2c, the product mainly has a novel dendritic structure. The orientation of dendrite is very unique. Each dendrite contains a main 'trunk' with some regular 'arrowhead' structures growing perpendicular to the major trunk. Typical SEM image of individual dendrite clearly reveals a view of its three-dimensional dendritic structure with two rows of arrowhead structures. The main trunk has the length of about 5 μm. The arrowhead structures have nearly similar morphology but they are different in size. The size of these structures decreases from tip to bottom of the dendrite. The higher magnification image (Fig. 2d) clearly indicates that these dendritic structures are composed of some small nanoparticles. Fenske et al. [24] suggested that the PbS grows firstly in the longitudinal direction, the ⟨100⟩ direction, to form the nanorod, and then grows laterally, the ⟨011⟩ direction, to form the dendrite at the temperature about 140 °C. The shape evolution of PbS observed in our experiment provides a good example of such processes.

When the reaction temperature raised to 170 °C (sample 4; Fig. 2e, f), the cubic PbS with edge length about 3 μm was gained. By increasing the reaction temperature to 170 °C, the preferential growth orientation along ⟨111⟩ rather than ⟨100⟩ led to the formation of cubes. As crystal growth proceeded, the size of the PbS crystals became larger, and thus the mass transport became much more

Table 1 Reaction conditions and characteristics of the samples prepared via hydrothermal method

Starting reagents	Surfactant	T (°C); t (h)	pH	Morphology	References
1. PbC$_2$O$_4$ + tu	TGA	110; 6		Microrod	Fig. 2a
2. PbC$_2$O$_4$ + tu	TGA	110; 18		Octahedral	Fig. 2b
3. PbC$_2$O$_4$ + tu	TGA	140; 18		Dendrite	Fig. 2c, d
4. PbC$_2$O$_4$ + tu	TGA	170; 18		Cubic	Fig. 2e, f
5. PbC$_2$O$_4$	TGA	170; 24		Octahedral	Fig. 2g
6. Pb(salicylaldehyde)$_2$ + tu	TGA	170; 18		Microleaf	Fig. 2h
7. PbC$_2$O$_4$	TGA/PEG	110; 6		Microrod	Fig. 4a
8. PbC$_2$O$_4$	TGA/PEG	140; 6		Microrod	Fig. 4b
9. PbC$_2$O$_4$ + tu	PEG	160; 18		Nanoparticle	Fig. 4c
10. PbC$_2$O$_4$	TGA	110; 7	6	Hexagonal disc	Fig. 5a, b
11. PbC$_2$O$_4$	TGA	110; 10	6	Microstar	Fig. 5c, d
12. PbC$_2$O$_4$	TGA	110; 6	7	Nanoparticle	Fig. 7a
13. PbC$_2$O$_4$	TGA	110; 6	10	Nanoparticle	Fig. 7b
14. PbC$_2$O$_4$	TGA	140; 6	7	Microstar	Fig. 7c
15. PbC$_2$O$_4$	TGA	140; 6	10	Irregular octahedral	Fig. 7d

Fig. 1 The XRD patterns of as-prepared PbS by reacting lead (II) oxalate and thiourea in the presence of TGA as surfactant at (*a*) 110 °C—6 h, (*b*) 170 °C—18 h
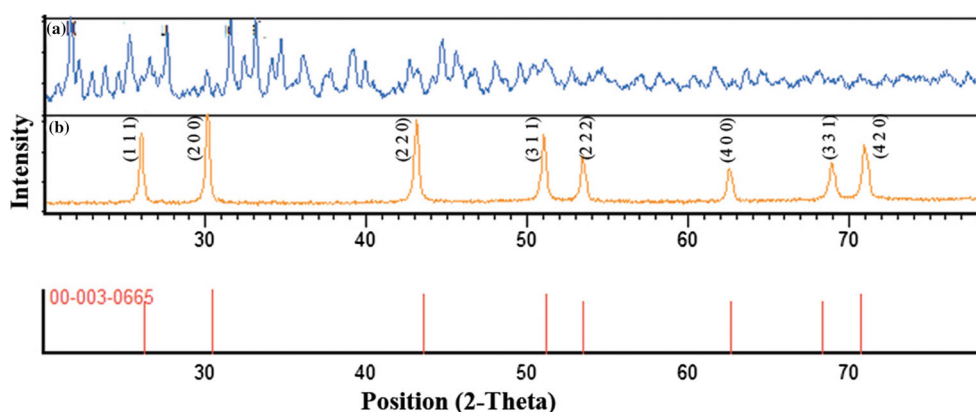
difficult, thereby resulting in the formation of eight-pod cubes of PbS (Fig. 2f) because of the Berg effect [25], that is, the growth rate of the edge of the {111} plane was faster than that of the {100} inner plane.

Thiourea, which slowly releases S^{2-} during its hydrolysis, could significantly affect the kinetic growth of PbS. In the absence of thiourea in 170 °C—24 h, octahedral structures with different sizes were formed (sample 5, Fig. 2g). The octahedral structures are formed due to the faster growth rates along ⟨100⟩ versus ⟨111⟩ directions. Nevertheless, a few cubic structures can be seen among the large number of the octahedral morphology (red circles in Fig. 2g).

For investigating the precursor effect, Pb(salicylaldehyde)$_2$ was used instead of PbC$_2$O$_4$ at 170 °C—18 h (sample 6, Fig. 2h). In the presence of Pb(salicylaldehyde)$_2$ as Pb^{2+} source, some microleaf structures with thickness about 400–500 nm were obtained. The surface of microleaves is rough, which implies that the outside of the leaf is composed of many nanoparticles.

To demonstrate the surface adsorption of the TGA on PbS microcrystals, FT-IR studies of PbS microcrystals, prepared in various times and temperatures, were performed. In the Fig. 3a, the typical bands at 3,514 (asym–OH stretching), 3,444 (sym–OH stretching), 2,875 (Sym–CH$_2$) and 1,585 cm^{-1} (C=O stretching) was revealed, proving the presence of the thioglycolic acid in the sample 1 [26, 27]. On the other hand, from the Fig. 3b it can be clearly seen that there is no characteristic peaks of TGA in the sample 5, which indicates that in higher temperature and time the TGA molecules removed from PbS particles during hydrothermal method. This further proves the desorption of TGA from the surface of PbS.

3.2 The surfactant effect

The kind of surfactant is one of the main factors that can affect the morphology of the final products. In the presence of PEG and TGA as surfactants at 110 °C—6 h (sample 7, Fig. 4a), uniform PbS microrods with diameter of about
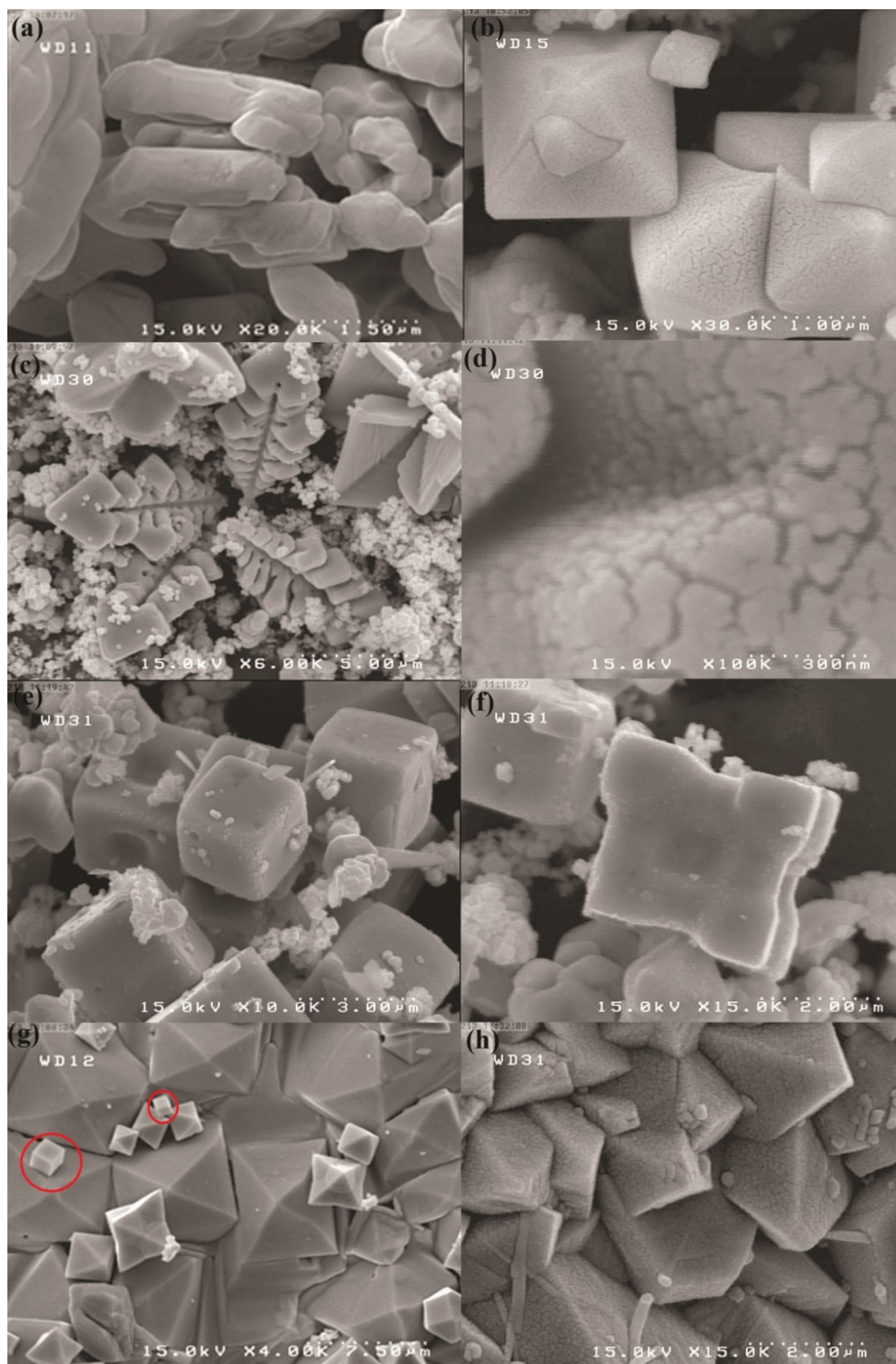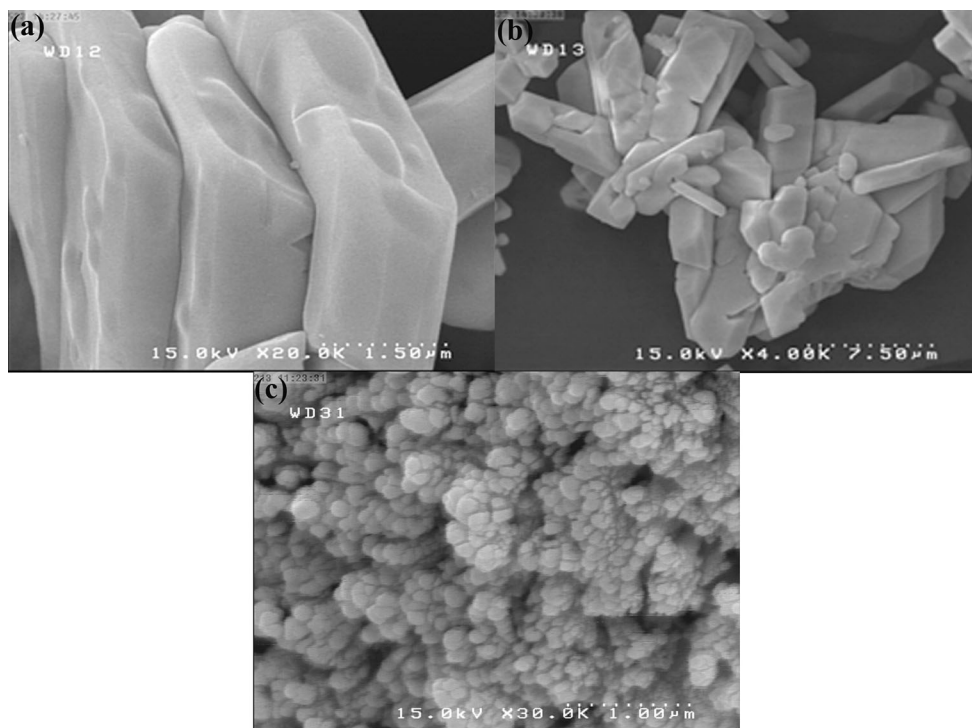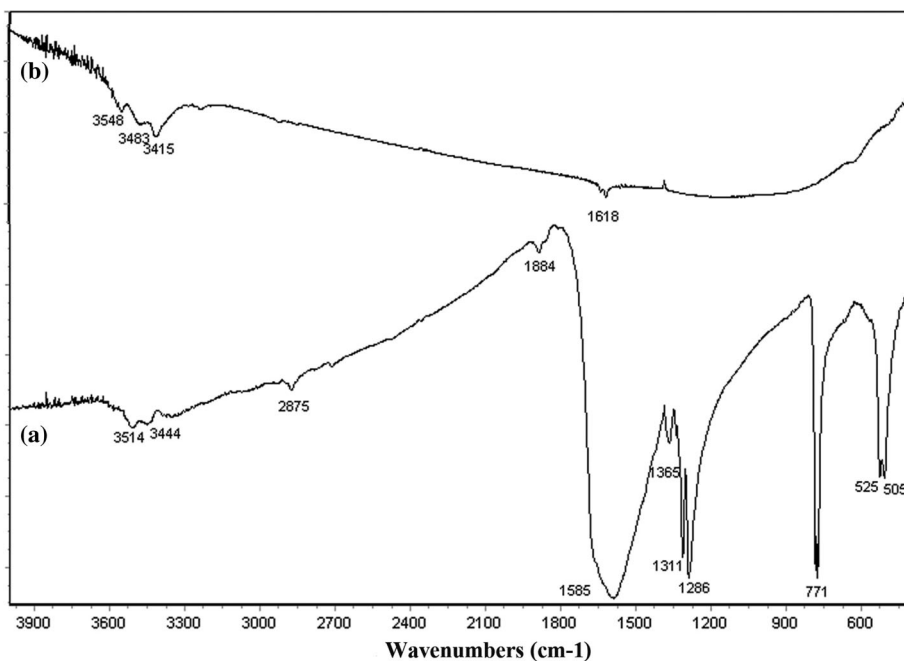
Fig. 2 The SEM images of as-prepared PbS using PbC_2O_4, tu and TGA at (**a**) 110 °C—6 h, (**b**) 110 °C—18 h, (**c**, **d**) 140 °C—18 h, (**e**, **f**) 170 °C—18 h, (**g**) without thiourea 170 °C—24 h and (**h**) with Pb(salicylaldehyde)$_2$ as precursor at 170 °C—18 h

1.5 µm were obtained. By increasing the reaction temperature to 140 °C (sample 8, Fig. 4b) broken microrods with various diameter and size were formed. By closer look at Fig. 4b some microparticles can be seen. It is known that

the intrinsic surface energy of the {111} faces containing only Pb^{2+} or S^{2-} is higher than that of {100} faces containing mixed Pb^{2+}/S^{2-}. Capping agent like PEG or TGA can selectivity stabilize the {111} surface by interacting

Fig. 3 The FT-IR spectra of as-prepared PbS using PbC_2O_4, tu and TGA at (*a*) 110 °C—6 h, (*b*) without tu 170 °C—24 h

Fig. 4 The SEM images of as-prepared PbS using PbC_2O_4, TGA and PEG at (**a**) 110 °C—6 h, (**b**) 140 °C—6 h, (**c**) PbC_2O_4, tu and PEG 160 °C—18 h

with the charged {111} faces rather than uncharged {100} faces, and accelerate the growth of {100} faces and microrods were deduced.

With changing the sulfur source to thiourea, in the presence of PEG as surfactant at 160 °C—18 h, uniform nanoparticles were obtained (sample 9, Fig. 4c). In higher times and temperatures, in the presence of thiourea, PEG was adsorbed on the surface of PbS in the nucleation stage and the surface energy was decreased. Therefore, the nanoparticles have enough stability to form.

3.3 The effect of pH

As a part of the study of the growth mechanism, the products of reaction at different pH were examined. As shown in the SEM images (Fig. 5a, b), hexagonal disc PbS structures were formed when lead (II) oxalate and TGA reacted at 110 °C for 7 h at pH 6 (sample 10). Although there is some variation in diameters, the thickness of the sheets is almost constant ∼550 nm. Schliehe et al. [28, 29] recently reported the preparation of 2D rectangular PbS sheets by oriented attachment of highly reactive ⟨110⟩ facets of small truncated cuboctahedron seeds. Also, hexagonal PbS discs were synthesized by Pandey et al. by reaction of lead (II) acetate and thiourea at pH 10 in hydrothermal conditions [30].

When the same reaction was performed at 10 h (sample 11), hierarchically 3D hyperbranched PbS microstars were formed (Fig. 4c, d). Each star has six main branches with length of about 3 μm, pointing to the six equivalent ⟨100⟩ directions of an imaginary octahedral (Fig. 4c). Each main branch supports four perpendicular rows referred to secondary branches with a diameter of ∼900 nm. The TEM image (Fig. 6) distinctly indicates the six petal of microstar PbS product. Moreover, the careful observation of microscopy images (Figs. 5d, 6) reveals that the petal of each star is composed of very tiny edge with diameter of about 30–40 nm. Furthermore, one can also detect the

presence of nanoparticles firmly attached to the surface of the structures.

In neutral and basic pH (sample 12, 13; Fig. 7a, b), irregular agglomerates of PbS were formed. The nanoparticles were clearly seen on the rough surface of irregular shapes. When the temperature was raised to 140 °C in neutral pH (sample 14, Fig. 7c), the six pod microstar was performed. Each star has six main branches with length of 2.5 μm. Also, on the each branch, arrowhead structures with different size can be seen. With increasing the pH of solution to 10 at 140 °C (sample 15, Fig. 7d), agglomerated nanoparticles with irregular morphologies were synthesized. Some irregular octahedral structures can be seen in the SEM image (red circles in Fig. 7d). The seed particles prefer to aggregate together to reduce the surface energy and microsphere of PbS was obtained.

In pH 6, due to preferential growth of smaller particles, star-like or hexagonal disc structures were obtained. In pH 10, the bonding between lead and thioglycolic acid is stronger than pH 6, therefore, lead ions are less available to react with sulfur source and nanoparticles were obtained instead of star-like nanostructure. The results show that in pH 10 nucleation overcome to preferential growth and nanoparticles were achieved.

The XRD patterns of two as-prepared PbS, samples 9 and 14, were shown in Fig. 8. The characteristic peaks of fcc PbS can be observed in the presence of PEG and tu at
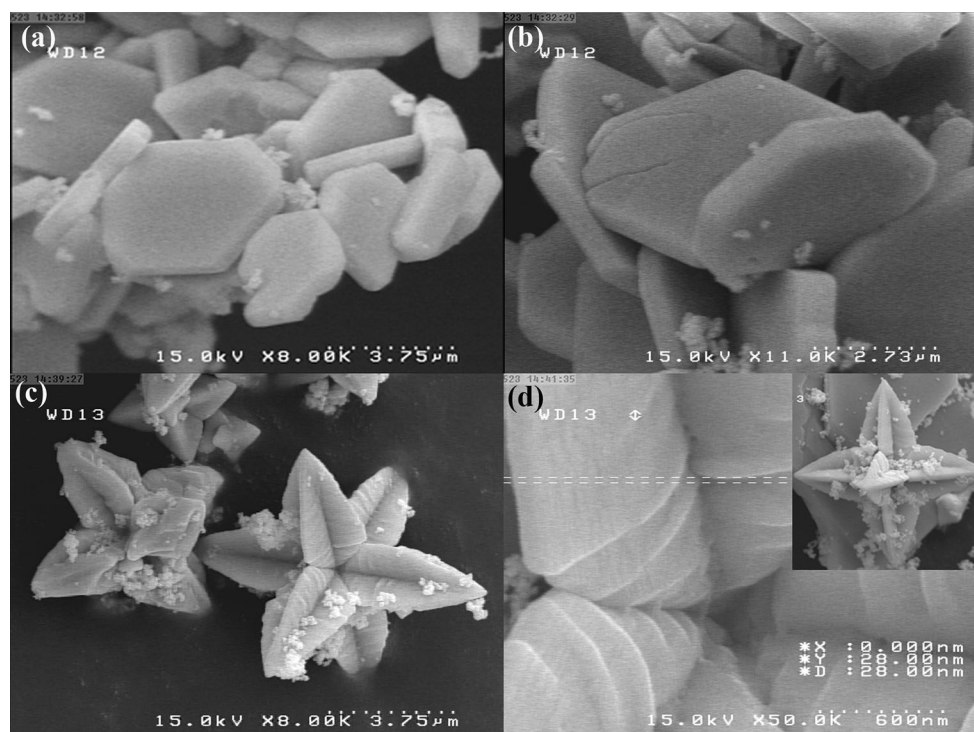
Fig. 5 The SEM images of as-prepared PbS using PbC_2O_4 and TGA at pH 6. (a, b) 110 °C—7 h, (c, d) 110 °C—10 h
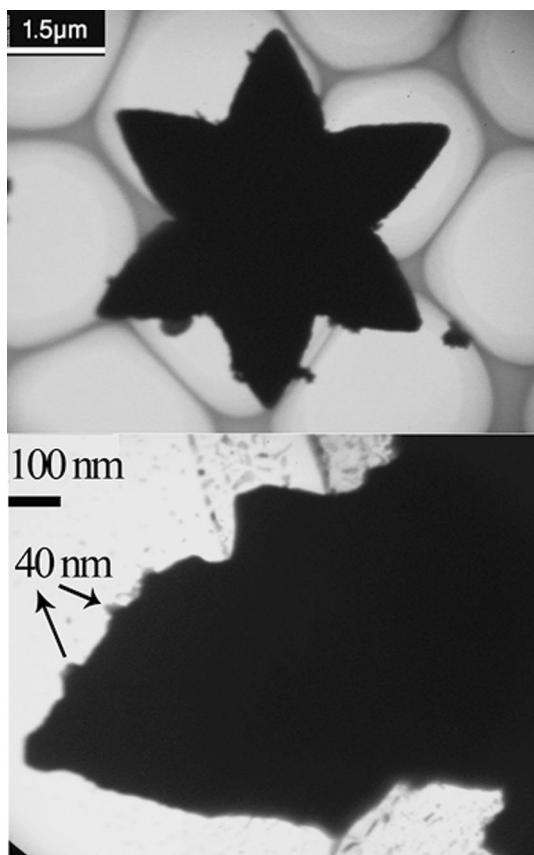
Fig. 6 The TEM images of as-prepared mictostar PbS using PbC_2O_4 and TGA at pH 6, 110 °C—7 h

160 °C—18 h, but some impurities are detectable (Fig. 8a). In lower reaction times and temperatures, in the presence of TGA at 140 °C—6 h and pH 7, the organic–inorganic composite was formed and the characteristic peaks of PbS can be seen hardly. According to Figs. 1 and 8, it is obvious that in lower temperatures and reaction times, the pure PbS phase was not crystalized truly, and an organic–inorganic composite was organized. By increasing the reaction times and temperatures a significant grain growth and better crystallinity can be seen.
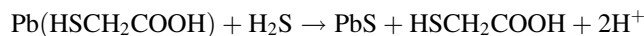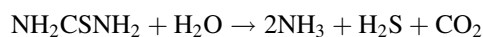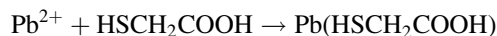
3.4 The general growth mechanism

Generally, the growth process of lead chalcogenide crystals includes two stages [31, 32]: the initial nucleation and a subsequent growth. During nucleation, the seeds crystallize as polyhedra, which exposes six {100} and eight {111} facets because of their highly symmetric cubic rock-salt crystal structures. At the growth stage, growth rates on different facets are determined by the surface energy. It is generally accepted that the difference between relative growth rates of the six {100} faces and the eight {111} faces of seeds with a truncated octahedron shape is

responsible for nanoscale geometries. The faster growth along the eight ⟨111⟩ directions perpendicular to {111} faces results in the elimination of such faces and subsequent formation of {100}-faceted cubes (Fig. 9). If the growth perpendicular to {100} faces is preferred, such faces eventually disappear and the resulting morphologies are eight-faced octahedra with {111} faces. If the latter growth is much faster than that along the ⟨111⟩ directions and longer growth times are allowed, six-branched star-shaped PbS is formed due to the growth along the six ⟨100⟩ directions of the octahedral structures (Fig. 9). On the other hand, if the faster growth along the eight ⟨111⟩ directions was continued, the octapod structures are formed.

Bashouti and Lifshitz [33] mentioned that the main environmental parameters that affect on the relative growth rate of different directions are as follows: (a) the stabilizing surfactants which can enhance or block the growth of specific facets, (b) the reaction temperature and duration which determine the choice of thermodynamic or kinetic growth, and (c) a large concentration of the precursors to enable a fast kinetic growth and Ostwald ripening effect. In a solution-phase synthetic process, impurities and surfactants are often used to alter the surface energies through adsorption or chemical interactions, and thus new shapes of the particles come into being. In a word, the final structure of a PbS crystal can be controlled by modulation of the ratio (R) between the growth rates in the ⟨100⟩ and ⟨111⟩ directions. As illustrated by Wang [34], the R for the formation of octahedra is 1.73, and that for the perfect cubes shape is 0.58.

In our study, TGA is used as capping agent. In aqueous solution, sulfur group of TGA can form complex with lead cation through coordination interaction, which greatly decreases the free Pb^{2+} ion concentration in solution. On the other hand, thiourea can react with water at certain temperature to produce H_2S:

$$Pb^{2+} + HSCH_2COOH \rightarrow Pb(HSCH_2COOH)$$

$$NH_2CSNH_2 + H_2O \rightarrow 2NH_3 + H_2S + CO_2$$

$$Pb(HSCH_2COOH) + H_2S \rightarrow PbS + HSCH_2COOH + 2H^+$$

Such a low concentration of cation and anion leads to a relatively slow nucleation rate and facilitates the growth of PbS nanocrystals in view of the dynamic process. During the growth stage, the reduction in surface energy is believed to be the primary driving force for simple particle growth.

3.5 UV–Vis and photoluminescence spectroscopies and optical properties of PbS

UV–Vis spectroscopy is a useful technique to monitor the optical properties of the quantum sized particles. The
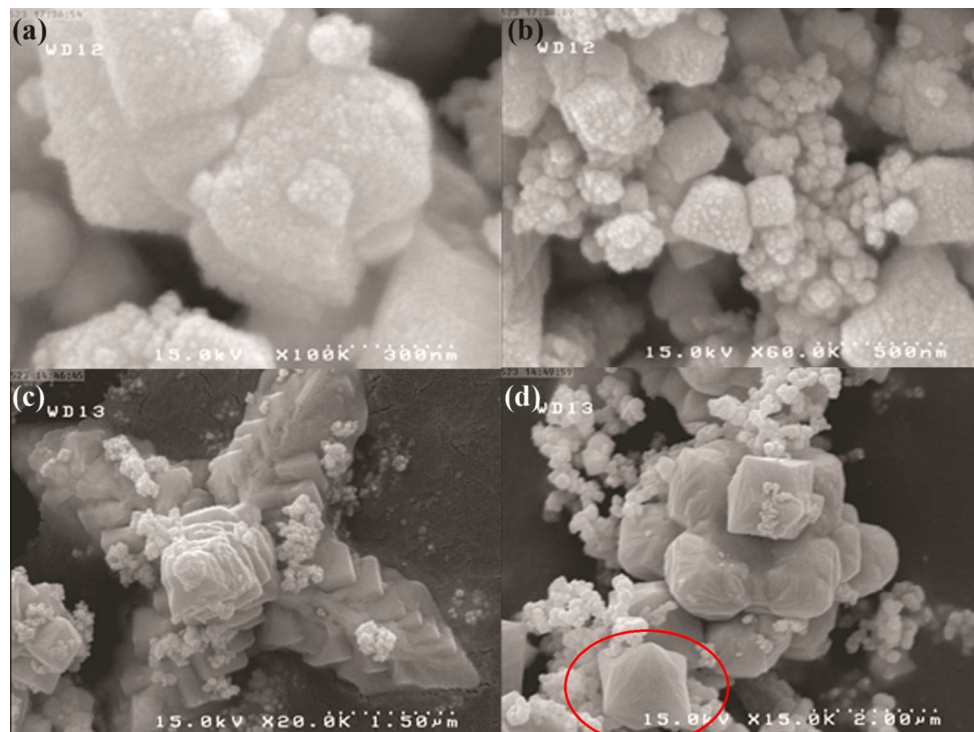
Fig. 7 The SEM images of as-prepared PbS using PbC_2O_4 and TGA at (**a**) 110 °C—6 h, pH 7, (**b**) 110 °C—6 h, pH 10, (**c**) 140 °C—6 h, pH 7, (**d**) 140 °C—6 h, pH 10

Fig. 8 The XRD patterns of as-prepared PbS using (*a*) PbC_2O_4, PEG and tu at 160 °C—18 h (sample 9), (*b*) PbC_2O_4 and TGA at 140 °C—6 h and pH 7 (sample 14)
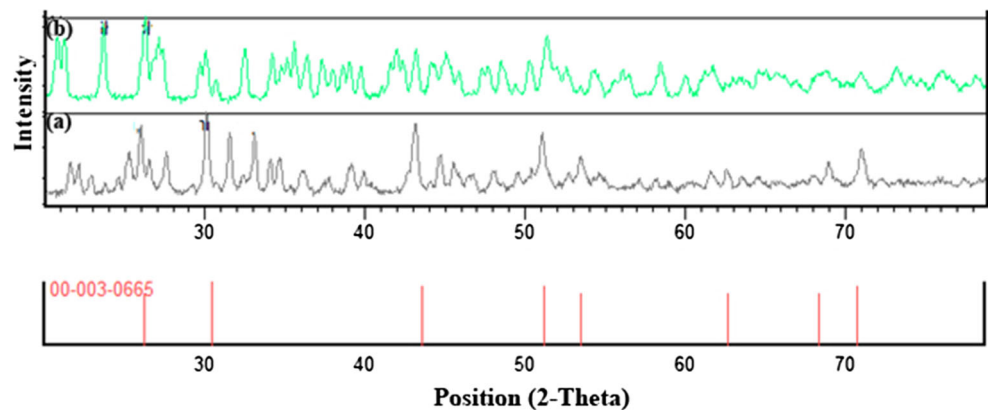
UV–Vis absorption spectrum of the as-synthesized micro-star PbS (sample 11) was shown in Fig. 10. The optical band gap energy of the products can be determined from the following equation:

$$\varepsilon h\upsilon = K(h\upsilon - E_g)^n$$

where h is the incident photon energy, K is a constant and E_g is the gap energy between the conduction and valance band of the nanoparticles. The $(\varepsilon h\upsilon)^{1/n}$ versus $h\upsilon$ plot for $n = 1/2$, shown in Fig. 11, indicates the presence of direct band gap in the as-prepared product. The optical band gap energy can be determined by extrapolating the curve to the energy axis for zero absorption coefficients. The optical band gap energy of PbS microstar has been estimated to be 5.8 eV which shows a large increment compared with that of bulk PbS (0.41 eV) [35, 36]. For other samples the band gap energy is in the ranges 4.5–5.8 eV.

The size of the PbS structures are larger than the Bohr radius of PbS (18 nm). The degree of the quantum confinement in the superstructure must be very small approaching the band gap of PbS in the bulk (0.41 eV). Such discrepancy must be related to nanoscale organization of the microstructure and thus, to its formation process. Usually, the decrease in the particle size results in

increasing the band gap and observation of blue shift. Although the sizes of PbS microstars are considerably larger than the exciton Bohr radius (18 nm) of PbS
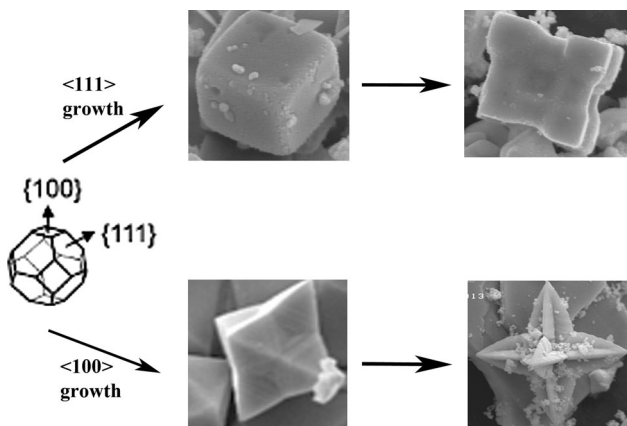
Fig. 9 Growth of truncated octahedral seeds containing six {100} and eight {111} crystallographic faces into (*first row*) cubic and eight-branched crystals (*second row*) octahedral and six-branched crystals
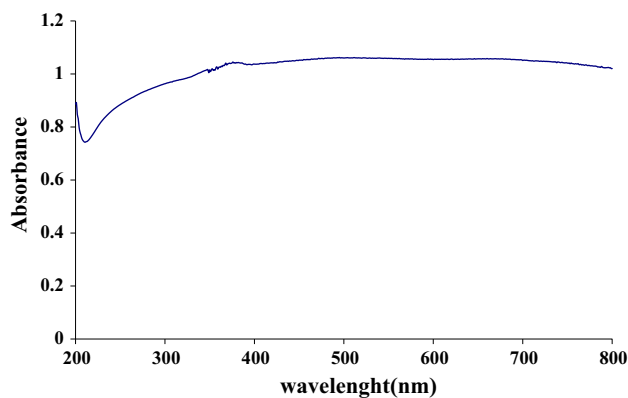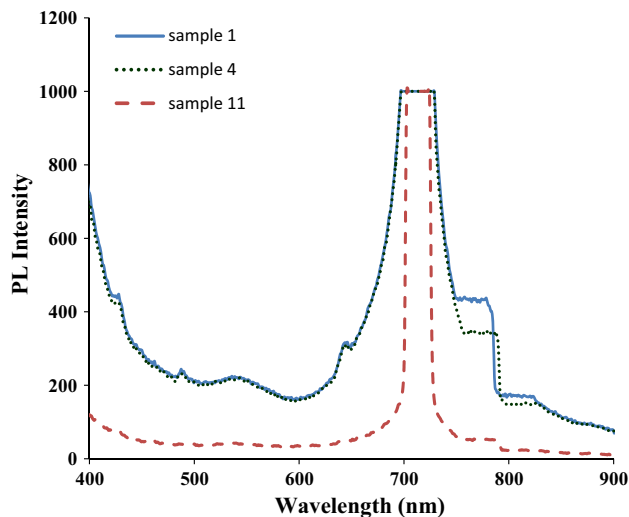

Fig. 10 UV–Vis spectrum of the as-prepared microstar PbS (sample 11)
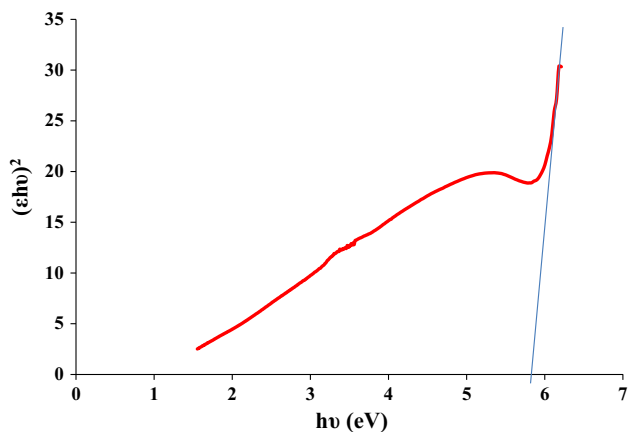
Fig. 11 Tauc plot of the as-prepared microstar PbS (sample 11)

nanocrystals, a large blue shift is observed in the band gap energy of the as-prepared PbS nanostructure compared with the bulk PbS. Such increment of band gap energy possibly occurs due to small effective mass of carriers in PbS. Cao et al. [37] also observed a large blue shift of the absorption edge in the UV region (5.04–4.57 eV) for their synthesized PbS nanocubes. Chattopadhyay et al. [8] reported the 4.9 eV band gap energy for tetrapods PbS product. The quantum confinement may occur near the tip edge of the PbS microstars, which are smaller or comparable to PbS Bohr radius. The band gap energy can also be increased from the inner thicker part to the tip edge of the crystal due to the position-dependent quantum-size effect [38].

Photoluminescence emission spectra of some of the prepared PbS samples are shown in Fig. 12. The samples kept at room temperature were excited with a light of wavelength 353 nm. The PbS bulk material has a small band gap (0.41 eV), which gives rise to emission at 3,024 nm. The PL spectra showed only one emission peak centered at 712 nm that exhibited a blue-shift relative to bulk PbS. The shift of the emission wavelengths from 3,024 [39] to 712 nm can be ascribed to a high level transition in PbS semiconductor crystallites. It has been reported that this kind of band edge luminescence arises from the recombination of excitons and/or shallowly trapped electron–hole pairs. The apparent blue-shift and the strong peak are also indicative of the size quantization attributed to quantum confinement of charge carriers in the restricted volume of the nanoparticles. The sharp luminescence is a dramatic example of the efficiency of the capping group in electronically passivating the crystallites [40].

Fig. 12 PL spectra of the as-prepared microstar PbS (sample 11)

4 Conclusions

In summary, different morphologies of PbS nano- and microstructures were synthesized by means of a quick and green hydrothermal method. Reaction time and temperature, the kind of surfactant and the pH of solution play an important role in the morphology of products. The shape evolution of PbS microcrystals can be controlled by the different growth ratio between the $\langle 111 \rangle$ and the $\langle 100 \rangle$ direction and the dissolution–recrystallization process. Evidently, the optical properties of PbS microcrystals is dependent on the morphology. The UV–Vis spectra of the PbS crystals showed a large shift in the band gap energy compared to bulk PbS crystals (0.41 eV). The PbS microstars offer a higher band gap than that of other morphologies. The product also showed a photoluminescence peak at 712 nm due to radiative recombination from the surface states. These PbS crystals may find potential applications in fundamental studies of nanostructure as well as for the fabrication of semiconductor devices based on these structures.

References

1. X. Peng, L. Manna, W. Yang, J. Wickham, E. Scher, A. Kadavanich, A.P. Alivisatos, Nature **404**, 59 (2000)
2. P. Gadenne, Y. Yagil, G.J. Deutscher, J. Appl. Phys. **66**, 3019 (1989)
3. F. Patolsky, G. Zheng, O. Hayden, M. Lakadamyali, X. Zhuang, C. Lieber, Proc. Natl. Acad. Sci. USA **101**, 14017 (2004)
4. R.S. Kane, R.E. Cohen, R. Silbey, J. Phys. Chem. **100**, 7928 (1996)
5. C.L. Lu, C. Guan, Y.F. Liu, Y.R. Cheng, B. Yang, Chem. Mater. **17**, 2448 (2005)
6. O. Hayden, R. Agarwal, C.M. Lieber, Nat. Mater. **5**, 352 (2006)
7. L. Bakueva, I. Gorelikov, S. Musikhin, X.S. Zhao, E.H. Sargent, E. Kumacheva, Adv. Mater. **16**, 926 (2004)
8. S. Jana, S. Goswamib, S. Nandya, K.K. Chattopadhyay, J. Alloy. Compd. **481**, 806 (2009)
9. N. Zhao, L.M. Qi, Adv. Mater. **18**, 359 (2006)
10. R. Hawaldar, U. Mulik, K. Patil, R. Pasricha, S. Sathaye, A. Lewis, D. Amalnerkar, Mater. Res. Bull. **40**, 1353 (2005)
11. G.J. Zhou, M.K. Lu, Z.L. Xiu, S.F. Wang, H.P. Zhang, Y.Y. Zhou, S.M. Wang, J. Phys. Chem. B **110**, 6543 (2006)
12. T. Trindade, P.O. Brien, X.M. Zhang, M. Motevalli, J. Mater. Chem. **7**, 1011 (1997)
13. J.M. Luther, H.M. Zheng, B. Sadtler, A.P. Alivisatos, J. Am. Chem. Soc. **131**, 16851 (2009)
14. S. Wang, S. Yang, Langmuir **16**, 389 (2000)
15. Y. Ma, L. Qi, J. Ma, H. Cheng, Cryst. Growth Des. **4**, 351 (2004)
16. Y. Ni, H. Liu, F. Wang, Y. Liang, J. Hong, X. Ma, Z. Xu, Cryst. Growth Des. **4**, 759 (2004)
17. D.B. Fan, P.J. Thomas, P.O. Brien, J. Am. Chem. Soc. **130**, 10892 (2008)
18. Y.L. Hou, H. Kondoh, T. Ohta, Cryst. Growth Des. **9**, 3119 (2009)
19. D. Yu, D. Wang, Z. Meng, J. Lu, Y. Qian, J. Mater. Chem. **12**, 403 (2002)
20. D. Yu, D. Wang, Z. Meng, J. Lu, Y. Qian, J. Cryst. Growth **249**, 195 (2003)
21. J. Xu, D.F. Xue, J. Phys. Chem. B **110**, 7750 (2006)
22. M. Salavati-Niasari, M.R. Loghman-Estarki, F. Davar, Inorg. Chim. Acta **362**, 3677 (2009)
23. Y. Liu, G. Xi, S. Chen, X. Zhang, Y. Zhu, Y.T. Qian, Nanotechnology **18**, 285605 (2007)
24. D.B. Kuang, A.W. Xu, Y.P. Fang, H.Q. Liu, C. Frommen, D. Fenske, Adv. Mater. **15**, 1747 (2003)
25. H.R. Liu, W.F. Miao, S. Yang, Z.M. Zhang, J.F. Chen, Cryst. Growth Des. **9**, 1733 (2009)
26. F. Davar, M. Mohammadikish, M.R. Loghman-Estarki, Cryst. Eng. Commun. **14**, 7338 (2012)
27. M. Mohammadikish, F. Davar, M.R. Loghman-Estarki, Z. Hamidi, Ceram. Int. **39**, 3173 (2013)
28. C. Schliehe, B.H. Juarez, M. Pelletier, S. Jander, D. Greshnykh, M. Nagel, A. Meyer, S. Foerster, A. Krnowski, C. Klinke, H. Weller, Science **329**, 550 (2010)
29. Z. Wang, C. Schliehe, T. Wang, Y. Nagaoka, Y.C. Cao, W.A. Bassett, H. Wu, H. Fan, H. Weller, J. Am. Chem. Soc. **133**, 14484 (2011)
30. G. Pandey, S. Shrivastav, H.K. Sharma, Phys. E **56**, 386 (2014)
31. T. Mokari, M.J. Zhang, P.D. Yang, J. Am. Chem. Soc. **129**, 9864 (2007)
32. T.J. Zhu, X. Chen, Y.Q. Cao, X.B. Zhao, J. Phys. Chem. C **113**, 8085 (2009)
33. M. Bashouti, E. Lifshitz, Inorg. Chem. **47**, 678 (2008)
34. Z.L. Wang, J. Phys. Chem. B **104**, 1153 (2000)
35. K.K. Nanda, F.E. Kruis, H. Fissan, M. Acet, J. Appl. Phys. **91**, 2315 (2002)
36. M.F. Acosta, M.S. Lerma, H.A. Chavez, F.F.C. Barraza, R.R. Bon, Solid State Commun. **128**, 407 (2003)
37. H. Cao, G. Wang, S. Zhang, X. Zhang, Nanotechnology **17**, 3280 (2006)
38. W.S. Chae, H.W. Shin, E.S. Lee, E.J. Shin, J.S. Jung, Y.R. Kim, J. Phys. Chem. B **109**, 6204 (2005)
39. E. Pintia, L. Pintilie, I. Matei, T. Botila, I. Pintilie, Infrared Phys. Technol. **44**, 207 (2003)
40. C.B. Murry, D.J. Norris, M.G. Bawendi, J. Am. Chem. Soc. **1158706**, 8706 (1993)